



HAL
open science

The Global Seismic Moment Rate of Mars After Event S1222a

M. Knapmeyer, S. Stähler, A. -C. Plesa, S. Ceylan, C. Charalambous, J. Clinton, N. Dahmen, C. Durán, A. Horleston, T. Kawamura, et al.

► **To cite this version:**

M. Knapmeyer, S. Stähler, A. -C. Plesa, S. Ceylan, C. Charalambous, et al.. The Global Seismic Moment Rate of Mars After Event S1222a. *Geophysical Research Letters*, 2023, 50, 10.1029/2022GL102296 . insu-04155749

HAL Id: insu-04155749

<https://insu.hal.science/insu-04155749v1>

Submitted on 7 Jul 2023

HAL is a multi-disciplinary open access archive for the deposit and dissemination of scientific research documents, whether they are published or not. The documents may come from teaching and research institutions in France or abroad, or from public or private research centers.

L'archive ouverte pluridisciplinaire **HAL**, est destinée au dépôt et à la diffusion de documents scientifiques de niveau recherche, publiés ou non, émanant des établissements d'enseignement et de recherche français ou étrangers, des laboratoires publics ou privés.



Distributed under a Creative Commons Attribution 4.0 International License

Geophysical Research Letters®







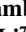


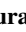

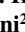
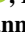
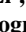
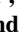

RESEARCH LETTER

10.1029/2022GL102296

Special Section:

The Large Marsquake of Sol 1222

The Global Seismic Moment Rate of Mars After Event S1222a

M. Knapmeyer¹ , S. Stähler² , A.-C. Plesa¹ , S. Ceylan² , C. Charalambous³ , J. Clinton⁴,
N. Dahmen² , C. Durán², A. Horleston⁵ , T. Kawamura⁶ , D. Kim², J. Li⁷, M. Plasman⁶,
G. Zenhäusern² , R. C. Weber⁸ , D. Giardini² , M. P. Panning⁹ , P. Lognonné⁶ , and
W. B. Banerdt⁹ 

¹DLR Institute for Planetary Research, Berlin, Germany, ²Institute of Geophysics, ETH Zürich, Zürich, Switzerland, ³Department of Electrical and Electronic Engineering, Imperial College London, London, UK, ⁴Swiss Seismological Service (SED), ETH Zurich, Zürich, Switzerland, ⁵School of Earth Sciences, University of Bristol, Bristol, UK, ⁶Université de Paris, Institut de physique du globe de Paris, CNRS, F-75005 Paris, France, ⁷Department of Earth, Planetary, and Space Sciences, University of California, Los Angeles, Los Angeles, CA, USA, ⁸NASA MSFC, Huntsville, AL, USA, ⁹Jet Propulsion Laboratory, California Institute of Technology, Pasadena, CA, USA

Key Points:

- A single large marsquake suffices to constrain the global seismic moment rate
- Pre-InSight estimations tended to overestimate the moment rate
- Either a significant part of the ongoing deformation occurs silent, or seismic activity is restricted to some activity centers, or both

Correspondence to:

M. Knapmeyer,
martin.knapmeyer@dlr.de

Citation:

Knapmeyer, M., Stähler, S., Plesa, A.-C., Ceylan, S., Charalambous, C., Clinton, J., et al. (2023). The global seismic moment rate of Mars after event S1222a. *Geophysical Research Letters*, 50, e2022GL102296. <https://doi.org/10.1029/2022GL102296>

Received 25 NOV 2022

Accepted 9 FEB 2023

Author Contributions:

Conceptualization: M. Knapmeyer, S. Stähler, J. Li, D. Giardini
Data curation: S. Stähler, S. Ceylan, C. Charalambous, J. Clinton, N. Dahmen, C. Durán, A. Horleston, T. Kawamura, D. Kim, M. Plasman, G. Zenhäusern, P. Lognonné
Formal analysis: M. Knapmeyer
Funding acquisition: D. Giardini, P. Lognonné, W. B. Banerdt
Investigation: A.-C. Plesa
Methodology: M. Knapmeyer
Project Administration: J. Clinton, R. C. Weber, D. Giardini, M. P. Panning, P. Lognonné, W. B. Banerdt
Software: M. Knapmeyer
Validation: M. Knapmeyer
Visualization: M. Knapmeyer

© 2023. The Authors.

This is an open access article under the terms of the [Creative Commons Attribution License](https://creativecommons.org/licenses/by/4.0/), which permits use, distribution and reproduction in any medium, provided the original work is properly cited.

Abstract The seismic activity of a planet can be described by the corner magnitude, events larger than which are extremely unlikely, and the seismic moment rate, the long-term average of annual seismic moment release. Marsquake S1222a proves large enough to be representative of the global activity of Mars and places observational constraints on the moment rate. The magnitude-frequency distribution of relevant Marsquakes indicates a *b*-value of 1.06. The moment rate is likely between 1.55×10^{15} Nm/a and 1.97×10^{18} Nm/a, with a marginal distribution peaking at 4.9×10^{16} Nm/a. Comparing this with pre-InSight estimations shows that these tended to overestimate the moment rate, and that 30% or more of the tectonic deformation may occur silently, whereas the seismicity is probably restricted to localized centers rather than spread over the entire planet.

Plain Language Summary The seismic moment rate is a measure for how fast quakes accumulate deformation of the planet's rigid outer layer, the lithosphere. In the past decades, several models for the deformation rate of Mars were developed either from the traces quakes leave on the surface, or from mathematical models of how quickly the planet's interior cools down and shrinks. The large marsquake that occurred on the 4th of May 2022 now allows a statistical estimation of the deformation accumulated on Mars per year, and thus to confront these models with reality. It turns out that, although there is a considerable overlap, the models published prior to InSight tend to overestimate the seismic moment rate, and hence the ongoing deformation on Mars. Possible explanations are that 30% or more of the deformation occurs silently, that is, without causing quakes, or that not the entire planet is seismically active but only specific regions.

1. Introduction

Seismic activity is an expression of current tectonic processes on a planet. A most obvious quantification is the number of seismic events, and their characterization in terms of magnitude. One of the science objectives of the SEIS instrument aboard InSight is indeed to “Determine the rate of seismic activity” of Mars (Lognonné et al., 2019).

Seismic moment is a measure of the permanent deformation associated with a quake, and magnitude is essentially its logarithm. Landforms of tectonic origin represent deformations accumulated in the past, and thus the cumulative seismic moment of many quakes. Comparing the current rate of accumulation with existing landforms thus connects past and present.

Up to 2020, all estimations of today's Martian moment rate were based on modeling or indirect evidence: the seismic data from Viking (Anderson et al., 1977; Goins & Lazarewicz, 1979), geological evaluation of surface structures (Golombek, 2002; Golombek et al., 1992; Taylor et al., 2013), or geodynamic modeling (Knapmeyer et al., 2006; Phillips, 1991; Plesa et al., 2018). Of the latter, Knapmeyer et al. (2006) and Plesa et al. (2018) aimed at delineating the entire plausible parameter space, rather than defining a most likely result.

A first estimation based on InSight data was presented by Banerdt et al. (2020), although in terms of a magnitude-frequency distribution rather than seismic moment rate. At that time, several extrapolation steps were

Writing – original draft: M. Knapmeyer, A.-C. Plesa, A. Horleston, J. Li, D. Giardini

Writing – review & editing: M. Knapmeyer

necessary to obtain a global annual event rate from 13 regional events. In this work we follow a different approach that avoids extrapolation as far as possible. Our goal is to estimate the global seismic moment rate.

2. Methods and Results

The events used for the estimation of the global seismic moment rate must be representative for the global endogenous seismicity, and hence comply with two criteria: They have to be detectable at any time, and they have to be detectable (with SEIS) from any location. The first criterion applies to the Signal-to-Noise ratio (SNR) at the site of the seismometer, the second criterion involves epicentral distance and therefore applies to the magnitude of the event. In addition, impacts and other non-tectonic events have to be discarded.

We use a catalog snapshot covering the time from 02 February 2019 to 06 July 2022 (1,190 terrestrial days) and containing 2,706 events. The first published catalog listing S1222a is the 12th catalog (InSight Marsquake Service, 2022) which covers the time up to 30 June 2022. Our snapshot has 6 additional but irrelevant SHF events (see catalog for type and quality class definitions). Two major instrument downtimes (28 August 2019 to 18 September 2019, and 07 January 2022 to 30 January 2022) and a number of data downlink interruptions reduce the effective observation time to 1,128 days. Magnitudes and their uncertainties are taken as listed in the catalog.

We discard all 1,696 quality “D” events which, by definition, are spurious detections that might represent wind gusts and other disturbances. We discard all 1,389 events of SHF type, which are considered to represent thermal cracking within the soil in the vicinity of the lander (Dahmen et al., 2020). We further discard events identified as impacts by Garcia et al. (2022), Kim et al. (2022), and Posiolova et al. (2022), 70 VHF events the nature of which is unclear and still under investigation, and 1,153 HF events. Although we consider the latter as predominantly tectonic (Stähler et al., 2022), we discard them a priori since they are so small that they would be discarded by magnitude and amplitude criteria anyway. Finally, 68 events from the “low frequency” (LF and BB) family remain for further analysis (squares in Figures 1a and 1b), 52 with known magnitudes.

2.1. Event Selection: Detectable at Any Time

We compute the noise root mean squared (RMS) ground displacement amplitude in consecutive windows of 2 min duration over the entire observation period. For convenience, we convert it into dB with respect to a reference displacement of 1 m. Due to the variability of wind speeds between seasons, and also between day and night (Charalambous et al., 2021), the RMS amplitude varies over a range of approx. 40 dB (Figures 1a and 1b). From the time series of RMS amplitudes, we compute the cumulative distribution function (CDF) of amplitudes (Figure 1c). This CDF is below -185.8 dB for 95% of the time. Evaluation of the distribution of the SNR ratio suggests that we detected all events with an SNR (from an STA/LTA detector used for event detection) exceeding 2, thus an allowance of about 6 dB on the noise level must be considered. A total of eight events exceeds the resulting threshold amplitude of -179.8 dB (S0173a, S1022a, S1133c, S1157a, S1157b, S1157c, S1197a, S1222a, above the horizontal dashed lines in Figures 1a and 1b), whereas event S0976a, with $\Delta = 146^\circ$ and a magnitude of 4.2 ± 0.3 (Horleston et al., 2022), was removed due to its SNR.

2.2. Event Selection: Detectable From Anywhere

For two of the eight remaining events, it was not possible to estimate the epicentral distance (quality “C” events). From the other six, we identify the one with the smallest recorded amplitude (S1197a). We convert this amplitude into the magnitude an event needs to have at any distance from 0° to 180° to be recorded with the observed amplitude, using the body wave magnitude equation of Böse et al. (2021). We thus obtain a detection threshold magnitude as function of distance (Figure 1d). Evaluating the equation for $\Delta = 180^\circ$, we find that an event with a magnitude of 4.1 ± 0.2 would be detectable anywhere on Mars, and, based on the events used to determine the threshold, during 95% of the time. In the following we assume a threshold of 4.1. It is remarkable that this is more than 2 magnitudes below the Anderson et al. (1977) estimation for Viking (with a short period seismometer installed on the lander platform).

Only one event, S1222a ($M_W = 4.7 \pm 0.2$; Kawamura et al., 2022), is above both amplitude and magnitude thresholds.

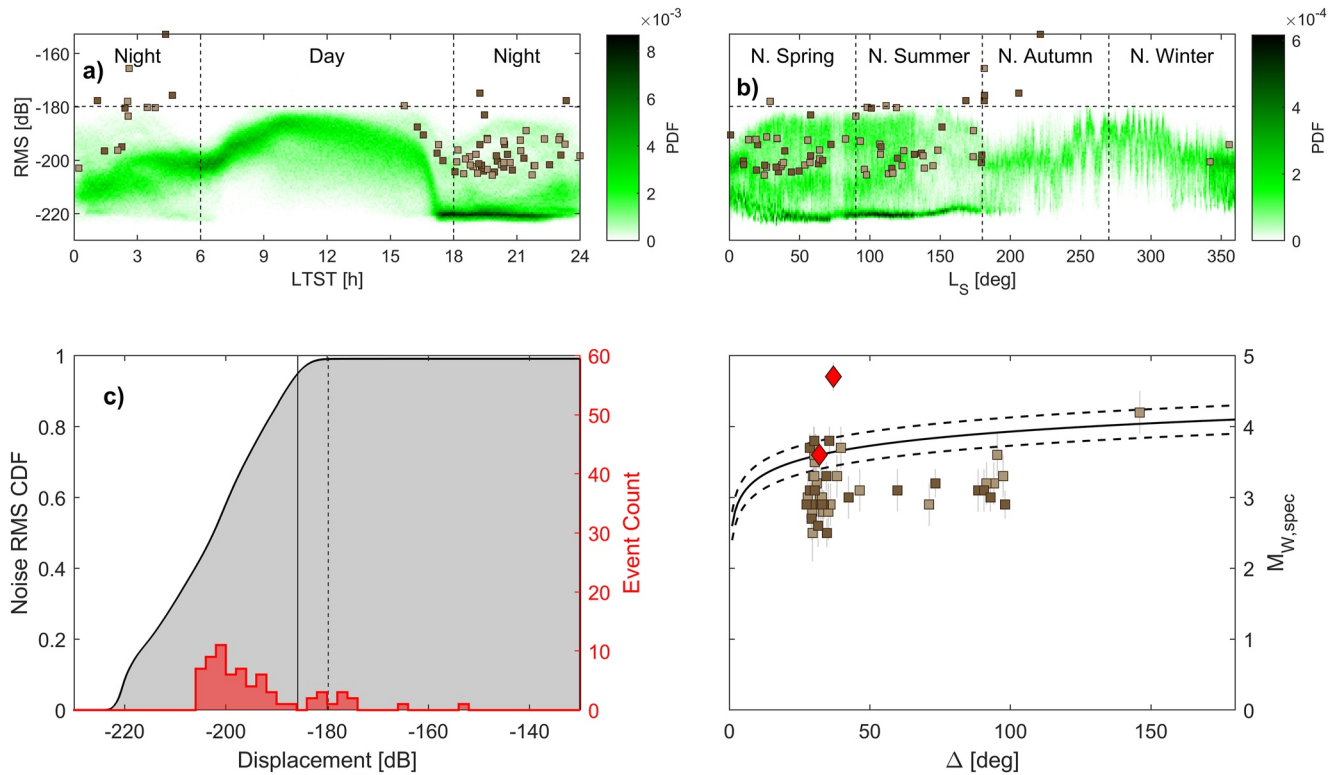


Figure 1. Event selection criteria. (a) Background: histogram of displacement RMS amplitudes throughout the sol (squares: LF (bright) and BB (dark) event amplitudes). Horizontal line: -179.8 dB. LTST: local sun clock time. (b) Background: displacement RMS amplitudes throughout the martian year, L_S : areocentric longitude of the Sun, symbols as in (a). (c) Gray: noise RMS cumulative distribution, red: histogram of event amplitudes in 2 dB bins. 95% of all noise amplitudes are left of the solid vertical line, the dashed vertical line marks -179.8 dB (i.e. SNR 2). (d) Event magnitudes (all 52), including their individual uncertainties (colors as in (a)) Solid curve: Amplitude of the weakest of the surviving eight events from (c) (S1197a, lower red diamond), converted to moment magnitudes for all distances. Dashed: as the solid curve, but factoring in the magnitude uncertainty. Upper red diamond is for S1222a.

2.3. b -Value and Moment Rate Estimation

With only one event left, we have to resort to the NLVR (Normalized Largest eVent eveR) estimator of Knapmeyer et al. (2019), which assumes that the cumulative moment-frequency distribution follows a tapered Gutenberg-Richter (TGR, Kagan, 2002) distribution with corner moment M_{\max} and magnitude of completeness M_c , such that the relative number Φ of events exceeding magnitude M is

$$\Phi(M) = \left(\frac{M_c}{M}\right)^\beta \exp\left(\frac{M_c - M}{M_{\max}}\right) \text{ for } M_c \leq M \leq \infty \quad (1)$$

When written as function of b -value, largest observed magnitude, M , and number of years, n , the moment rate \dot{M} is estimated as

$$\dot{M} = \frac{1}{n} \frac{\Gamma(2 - 2b/3)}{1 - 2b/3} 10^{9.1+3M/2} \quad (2)$$

where $\Gamma(x)$ is the gamma function. The magnitudes listed in the MQS catalog are calibrated as moment magnitudes (Böse et al., 2021), and standard deviations are reported. With $\sigma_m = 0.2$ for S1222a, the magnitude uncertainty amounts to factors of 0.5 and 2 in seismic moment, respectively.

To estimate b , we use all 52 low frequency events with known magnitudes and propagate their magnitude uncertainties: We first produce a number of perturbed magnitude lists, where a random perturbation is added to each magnitude entry to account for the magnitude roundoff and the cataloged magnitude uncertainty. For each of the perturbed catalogs, we evaluate a modified version of the well-known maximum-likelihood solution for b ,

$$b = \frac{\log_{10} e}{\bar{m} - (M_c - \delta m/2)} \quad (3)$$

where

$$\bar{m} = \frac{1}{N} \sum_{i=1}^N M_i \quad (4)$$

for the $N = 52$ cataloged events with magnitudes above the magnitude of completeness. Instead of estimating M_c from the catalog, we simply increment it from a value that is certainly too low to the largest value that still allows to evaluate the standard deviation of b after Shi and Bolt (1982), which is undefined for less than three events. We assume with Cao and Gao (2002) that the resulting b -curve will form a plateau when the assumed M_c exceeds the true value, but we don't think that the evaluation of the formal uncertainty of b is a meaningful criterion to identify the plateau with a catalog as small as ours. Instead, we define a reasonable interval $2.9 \leq M_c \leq 3.3$ by visual inspection of Figure 2c, and analyze the distribution of b -values resulting from our ensemble for perturbed catalogs for M_c within that interval.

The mentioned modification of the maximum likelihood solution accounts for the fact that almost all events would be undetectable at typical daytime noise levels. Taking the catalog as-is would probably underestimate the b value, as predominantly the small events are missing from the catalog and thus the small-events end of the magnitude-frequency distribution is biased toward low counts. We account for this by upweighting small events.

For each given event, the reciprocal of the cumulative distribution of the noise RMS amplitude, $CDF(A)$ (Figure 1c), indicates during how much of the time it would have been detectable. A simplistic way to mitigate the lack of events would be to insert a number of artificial entries to increase the number of small events and then evaluate this mended catalog. A more precise way is to replace the arithmetic mean \bar{m} in Equation 3 with a weighted mean

$$\tilde{m} = \frac{1}{\hat{N}} \sum_{i=1}^N g_i M_i \quad (5)$$

where $\hat{N} = \sum_{i=1}^N g_i = 82.86$, and

$$g_i = \frac{1}{CDF(A_i)} \quad (6)$$

with the amplitude A_i of the i -th event. The weights g_i range from 1.01 to 2.04 (Figure 2a). When evaluating the formal standard deviation, \hat{N} has to be used instead of N as well. This modification corrects for the loss of events during high noise times. We do not attempt to correct for undetectably small events at large distances also missing from the catalog, since we lack the necessary information.

Each magnitude listed in the catalog carries an individual uncertainty, which is assumed to be normally distributed. This leads to an uncertainty of the number of events exceeding any given magnitude and thus propagates into b (Figure 2b). To account for this, we evaluate not only the nominal magnitudes of the catalog, but also a large number of perturbed catalogs, where each magnitude entry is modified with a random offset drawn from a normal distribution with the standard deviation reported for the individual events (Figure 2b). We do not show the formal standard deviation of b here, which grows hyperbolically toward the right of Figure 2c, when the number of events used decreases. The width of the b -value distribution in Figure 2c roughly corresponds to three formal σ .

From all b -values entering the plateau region of Figure 2c (from 2.9 to 3.3, between the heavy dashed verticals), we finally obtain a PDF of b values (Figure 2d) which has its maximum at $b = 1.06$ (mean $\bar{b} = 1.105$; $\sigma_b = 0.152$). We tentatively use magnitudes 3.1 and 3.5 as the right end of the plateau region in Figure 2c, yielding b -values of 1.03 and 1.07, respectively, showing that the dependence on this choice is weak compared to the width of the PDF, and comparable to the uncertainty of reading the maximum location from a histogram. Since the dependence of the moment rate estimation on b is also weak (see Equation 2, and Knapmeyer et al., 2019), we proceed with $b = 1.06$ for an upper threshold of 3.3, which we consider most plausible. We note that a b -value below 1 is much more likely than one above 1.5 (26% vs. 1.4%, Figure 2d).

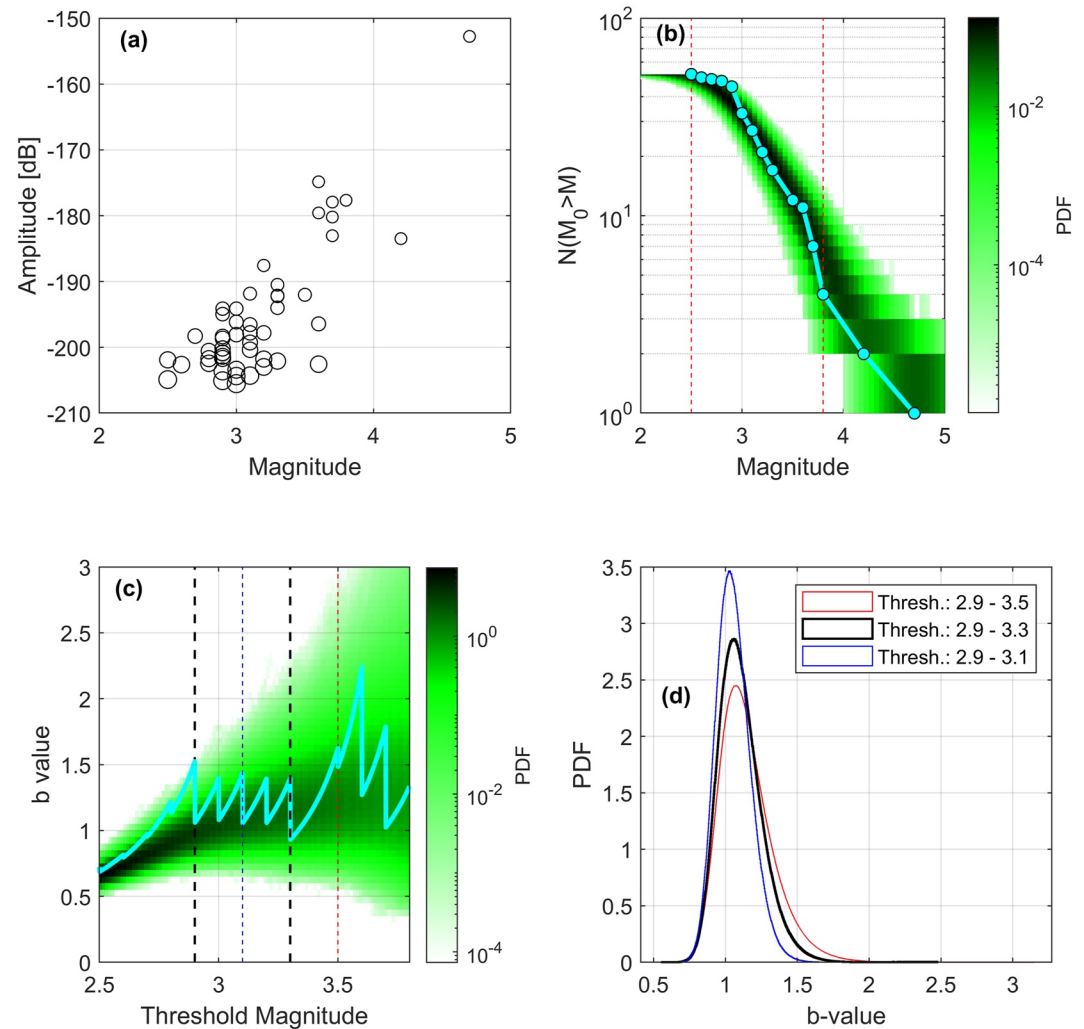


Figure 2. *b*-value estimation. (a) Amplitude-dependent weights of each event; symbol area is proportional to weight. (b) Cumulative magnitude distribution. Line and circles: catalog values. Background: 100,000 random perturbations of catalog magnitudes. Dashed lines: scan interval for assumed magnitude of completeness. (c) Line: *b*-value curve resulting from catalog magnitudes. The sawtooth shape results from stepwise reduction of included events. Background: PDF of curves resulting from catalog perturbations. Vertical dotted lines: Plateau zone of near constant *b*. (d) Distribution of *b*-values from within the plateau zone of (c) as indicated in legend.

We now have all parameters for the evaluation of Equation 2 at hand. Inserting $n = 1,128/365.25$, $M = 4.7$, and $b = 1.06$, we obtain $\dot{M} = 1.4 \times 10^{16}$ Nm/a (where a refers to terrestrial years), and the magnitude uncertainty $\sigma_m = 0.2$ results in upper and lower bounds

$$7.0 \times 10^{15} \text{ Nm/a} \leq \dot{M} \leq 2.8 \times 10^{16} \text{ Nm/a} \quad (7)$$

The catalog is only one realization of a random process drawing from the moment-frequency distribution, which also depends on the corner moment. We need to estimate how the probability to obtain the observed moment rate after ≈ 3 years depends on the choice of *both* parameters of the TGR distribution, and how the parameters trade off against each other.

To this end, we scan the parameter space defined by \dot{M} and M_{\max} on a regular grid, where both parameters are expressed as equivalent magnitudes according to $M_w = (\log_{10} M_0 - 9.1) \times 2/3$. For a given *b*-value, each node of this grid defines a TGR. We generate 2,000 synthetic event TGR catalogs per node and evaluate Equation 2, to obtain a distribution of NLVR estimations. These estimations are compared with the above intervals to obtain the desired probabilities, called emission probabilities by Knapmeyer et al. (2019). Figure 3 shows these

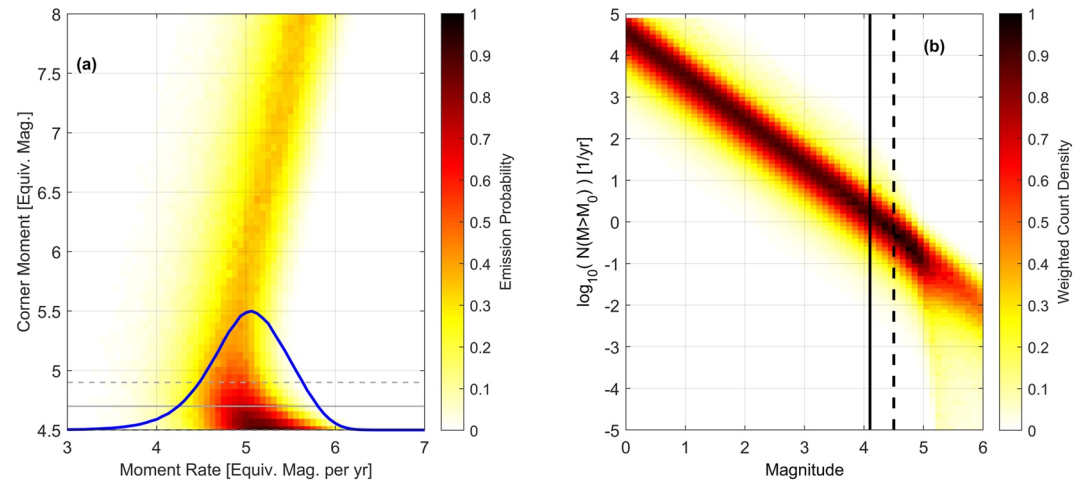


Figure 3. Feasible combinations of moment rate and corner moment, converted to magnitudes. (a) Emission probabilities as function of moment rate and corner moment, estimated from 2,000 synthetic catalogs per pixel. Horizontal lines indicate the magnitude of S1222a and its uncertainty. At the bottom: marginal emission probability as function of moment rate. (b) Density of TGR function graphs, weighted by emission probability.

probabilities in the moment-rate-corner-magnitude parameter space and in the form of the corresponding cumulative size-frequency distributions.

Most parameter combinations are very unlikely to produce the NLVR moment rate intervals of Equation 7 (white in Figures 3a and 3c), this includes the “Medium,” “StrongFew” and “StrongMany” models of Knapmeyer et al. (2006).

Feasible parameter combinations are found in the colored region of Figures 3a and 3c, which also includes the “WeakMany” (emission probability 73%) and “WeakFew” (15%) of Knapmeyer et al. (2006). We set an arbitrary cutoff for our grid search at $M_{\max} = 8$, but it is easy to extrapolate to higher values at will. Toward low corner moments, we set a cutoff at the lower bound of the magnitude uncertainty of S1222a, that is, at $M_{\max} = 4.5$. An even lower value of M_{\max} would imply that we already saw the largest event possible on Mars - it is safe to assume that we didn't.

The highest emission probabilities are found for corner moments below the mean magnitude of S1222a and moment rates slightly above having one event like S1222a per year.

The marginal distributions (from summation over the corner moments) at the bottoms of Figure 3a indicates the moment rate which most likely reproduces the observed NLVR range. When requiring a minimum emission probability of 0.1, the moment rate is bounded upwards by an equivalent magnitude of 6.31 (3.7×10^{18} Nm/a), whereas a moment rate equivalent of 5.06 (4.9×10^{16} Nm/a) is most likely to reproduce the observation. The marginal distribution does not rule out a moment rate below that of the Shallow Moonquakes (3.8), although this is very unlikely. Emission probabilities above 10% are found only for moment rates between equivalent magnitudes of 4.06 (1.55×10^{15} Nm/a) and 6.13 (1.97×10^{18} Nm/a). A higher upper bound would imply to consider possible Marsquakes with magnitudes above 8. Even Cerberus Fossae, which appears to be the seismically most active region at least on the InSight hemisphere of Mars, does currently not make us expect events of this size (see also Stähler et al., 2022), although the longest grabens on Mars are long enough to accommodate magnitude nine events (according to the Knapmeyer et al., 2006, fault catalog).

Figure 3b shows the density of TGR function graphs in magnitude-frequency coordinates, with each distribution weighted by its emission probability, and normalized to the density maximum. Here, small M_{\max} values result in steep slopes at magnitudes above 5, while the unconstrainedness of M_{\max} also allows distributions where the exponential taper has no effect within the depicted magnitude range.

The increasing dust load on InSight's solar arrays made continuous operation of SEIS increasingly difficult in 2022. A 10 sols data gap begins two sols after S1222a: Under slightly different weather conditions we might

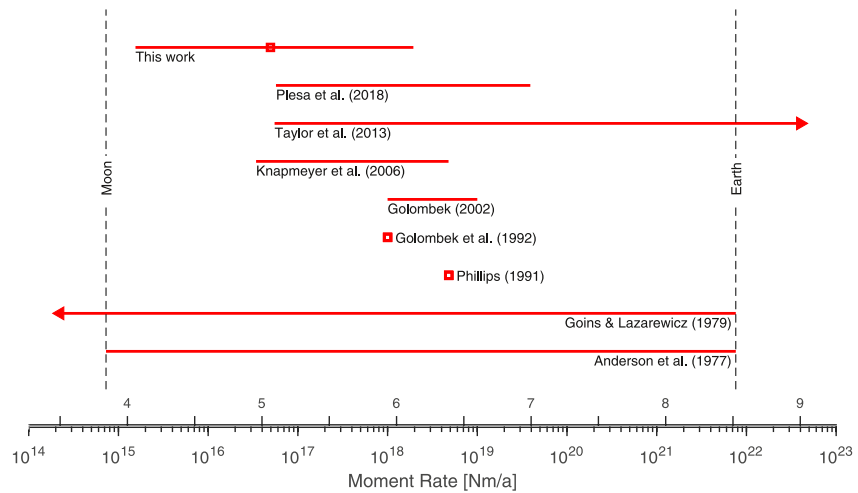


Figure 4. Comparison of published moment rate estimations. Earlier estimations either give intervals (horizontal bars, with an arrowhead if no bound in one direction was given) or single values (squares). Our result is depicted as the interval for which the emission probability exceeds 10%, and the maximum of the marginal distribution is indicated by a square. Values for Earth and Moon from Knapmeyer et al. (2019). Rulers give the moment rate in Nm/a and as equivalent moment magnitude.

have missed this event altogether. We repeat our analysis under the assumption that S0976a, although marginally below our acceptance thresholds, is still the largest observed event by July 2022. As expectable with the larger magnitude uncertainty of S0976a, we obtain a wider rate range with emission probabilities above 10% (3.4–6.5 in terms of magnitude). The smaller magnitude of S0976a makes the marginal distribution peak at a smaller rate (4.6). This result may also serve as guideline for rate estimation changes to expect from improved magnitude estimations for S1222a.

3. Discussion

Compared to pre-InSight estimations (Figure 4), our moment rate is in the middle to lower part of their intervals, and even below those: All earlier publications tended to overestimate the moment rate. For some cases, this is easily explained by the discrepancy between geodetically observable and seismic deformation: only some fraction of all tectonic deformation causes quakes, even on Earth. The seismic moment rate only reflects brittle, but not ductile deformation, whereas a reconstruction of crustal deformation from geologic mapping also includes the latter.

This applies to the estimations of Golombek et al. (1992), Golombek (2002), and Taylor et al. (2013). The latter estimated the moment rate of the Cerberus Fossae formation only but did not define an upper bound for the planetary moment rate.

The Viking non-observation of seismicity did not allow deriving tight constraints. The resulting estimations (Anderson et al., 1977, and further detailed by Goins & Lazarewicz, 1979) were both focused on event rate rather than moment rate.

One might of course argue that the Earth's moment rate (and the derived event rate) must be larger than that of Moon and Mars just because of the planet's sizes.

The appropriate framework for a size-dependent moment rate scaling is the equation of Kostrov (1974, see also Bratt et al., 1985), which also underlies the predictions for Mars from thermal evolution models. According to this equation, the moment rate is proportional to strain rate and seismogenic volume—which is not easy to determine. In terrestrial oceanic crust, the seismic nucleation depth appears to be limited by the 600°C isotherm (Abercrombie & Ekström, 2001; McKenzie et al., 2005), so one could estimate the seismogenic volume of oceanic crust from thermal models thereof for the entire surface covered by it. Kreemer et al. (2000) however show that a much smaller volume derived from the world strain map suffices to explain the Earth's seismic moment rate from observed strain rates.

Our knowledge of nucleation depths on the Moon appears patchy, at best, when comparing the source depths of shallow moonquakes found by different authors (e.g., Knapmeyer & Weber, 2015, and references therein). Little do we know about Mars, but enough to conclude that when taking the entire lithosphere above the 600°C isotherm, the resulting volume would exceed the Kreemer et al. volume for the Earth, whereas taking the source depth estimations of Brinkman et al. (2021) and Jacob et al. (2022), which are 40 km or less, as upper limit, the resulting volume would be smaller than what we get for the Moon with a seismogenic depth of 300 km. We therefore think that our knowledge is insufficient to derive a proper scaling relation between the Moon, Mars, and the Earth. Taken in absolute terms, the moment rates of Moon and Earth turn out as valid brackets for the Martian one, nevertheless.

Phillips (1991), Knapmeyer et al. (2006), and Plesa et al. (2018) based their estimations on increasingly complex thermal evolution models. Knapmeyer et al. (2006) introduced a seismic efficiency factor η to decouple brittle and ductile deformation, but only crude estimations of this factor could be made, which did not change with Plesa et al. Both did not expect the lowest moment rates we must consider possible after 3 years of InSight observations.

Without additional constraints, a low rate can still be attributed to a low seismic efficiency. In the model of Knapmeyer et al. (2006), as long as the seismogenic lithosphere is thin (less than about 300 km) the moment rate \dot{M} is proportional to shear modulus ($\mu = 30 \dots 70$ GPa), cooling rate ($\dot{T} = (0.2 \dots 1.1) \times 10^{-7}$ K/a), thermal expansion coefficient ($\alpha = (2 \dots 3) \times 10^{-5}$ 1/K), seismogenic lithosphere thickness ($h = 40 \dots 150$ km), and $\eta = 0 \dots 1$, that is, $\dot{M} \propto \eta \mu \alpha h \dot{T}$. Within the above parameter ranges of Knapmeyer et al. (2006), the only way to have a moment rate of 4.9×10^{16} Nm/a or less (i.e., below the rate at which the marginal emission probability has its maximum) is indeed if $\eta \leq 0.7$, or if the seismogenic volume is limited to a few active centers rather than comprising the entire planet - which is also plausible in the light of InSight's observations. Accordingly, the “StrongFew,” “StrongMany,” and “Medium” models of Knapmeyer et al. (2006) are all excluded by having emission probabilities below 3×10^{-4} .

Knapmeyer et al. (2006) considered their model parameters as independent of each other, which is not necessarily true. How to reconcile our moment rate with more complex thermal evolution models with realistic dependencies between parameters, will be investigated in the future.

4. Conclusions

In our estimation of the seismic moment rate of Mars, we avoided extrapolations from low noise to high noise times, and from regional to global seismicity by downselecting the recorded events to those detectable at any time and from anywhere. Unfortunately, only one event remained. Different approaches that make use of more of the detected events are possible, but will need extra assumptions and thus add extra tradeoffs. The single event nevertheless allowed deriving a feasible range of rates, which led us to the conclusion that pre-InSight publications, geologically or theoretically motivated, tended to overestimate the seismic moment rate. Our preferred explanation for this is that either aseismic deformation occurs, or the global seismogenic volume is restricted to some centers of activity (like Cerberus Fossae) and much smaller than previously assumed, or some combination of both as known from Earth. In the future, a seismic network on Mars, but also a precise geodetic monitoring of fixed points on the surface, may help to disentangle the two effects and further clarify the tectonic processes occurring not in a distant past but today.

Data Availability Statement

The InSight seismic event catalog version 12 (InSight Marsquake Service, 2022), the waveform data and station metadata are available from the Institut de Physique du Globe de Paris (IPGP) Datacenter and Incorporated Research Institutions for Seismology Data Management Center (IRIS-DMC; http://dx.doi.org/10.18715/SEIS.INSIGHT.XB_2016), as are the previous catalog versions. Seismic waveforms are also available from the National Aeronautics and Space Administration Planetary Data System (NASA PDS, <https://pds.nasa.gov/> (<http://doi.org/10.17189/1517570>)).

Acknowledgments

The authors gratefully acknowledge the advice of Maren Böse, ETH Zürich, concerning the treatment of magnitude uncertainties. The authors are also grateful to an anonymous reviewer whose questions and suggestions helped to improve our manuscript. The authors acknowledge NASA, CNES, partner agencies and Institutions (UKSA, SSO, DLR, JPL, IPGP-CNRS, ETHZ, IC, MPS-MPG) and the operators of JPL, SISMOC, MSDS, IRIS-DMC and PDS for providing SEED SEIS data. N.D., C.D., and G.Z. would like to acknowledge support from ETH through the ETH+ funding scheme (ETH+02 19-1: "Planet Mars"). M.P.P. and W.B.B. were supported by the NASA InSight mission and funds from the Jet Propulsion Laboratory, California Institute of Technology, under a contract with the National Aeronautics and Space Administration (80NM0018D0004). A.H. is funded by the UKSA under Grants ST/R002096/1 and ST/W002523/1. A.-C.P. gratefully acknowledges the financial support and endorsement from the DLR Management Board Young Research Group Leader Program and the Executive Board Member for Space Research and Technology. This is InSight Contribution ICN 273. Open Access funding enabled and organized by Projekt DEAL.

References

- Abercrombie, R. E., & Ekström, G. (2001). Earthquake slip on oceanic transform faults. *Nature*, *410*(6824), 74–77. <https://doi.org/10.1038/35065064>
- Anderson, D. L., Miller, W. F., Latham, G. V., Nakamura, Y., Toksöz, M. N., Dainty, A. M., et al. (1977). Seismology on Mars. *Journal of Geophysical Research*, *82*(28), 4524–4546. <https://doi.org/10.1029/jg082i028p04524>
- Banerdt, W. B., Smrekar, S. E., Banfield, D., Giardini, D., Golombek, M., Johnson, C. L., et al. (2020). Initial results from the InSight mission on Mars. *Nature Geoscience*, *13*(3), 183–189. <https://doi.org/10.1038/s41561-020-0544-y>
- Böse, M., Stähler, S. C., Deichmann, N., Giardini, D., Clinton, J., Lognonné, P., et al. (2021). Magnitude scales for marsquakes calibrated from InSight data. *Bulletin of the Seismological Society of America*, *111*(6), 3003–3015. <https://doi.org/10.1785/0120210045>
- Bratt, S. R., Bergman, E. A., & Solomon, S. C. (1985). Thermoelastic stress: How important as a cause of earthquakes in young oceanic lithosphere? *Journal of Geophysical Research*, *90*(B12), 20149–20260.
- Brinkman, N., Stähler, S. C., Giardini, D., Schmelzbach, C., Khan, A., Jacob, A., et al. (2021). First focal mechanisms of marsquakes. *Journal of Geophysical Research: Planets*, *126*(4). <https://doi.org/10.1029/2020JE006546>
- Cao, A., & Gao, S. S. (2002). Temporal variation of seismic b-values beneath northeastern Japan island arc. *Geophysical Research Letters*, *29*(9), 1334–1348-3. <https://doi.org/10.1029/2001GL013775>
- Charalambous, C., Stott, A. E., Pike, W. T., McClean, J. B., Warren, T., Spiga, A., et al. (2021). A comodulation analysis of atmospheric energy injection into the ground motion at InSight, Mars. *Journal of Geophysical Research: Planets*, *126*(4), e2020JE006538. <https://doi.org/10.1029/2020JE006538>
- Dahmen, N. L., Clinton, J. F., Ceylan, S., van Driel, M., Giardini, D., Khan, A., et al. (2020). Super high frequency events: A new class of events recorded by the InSight seismometers on Mars. *Journal of Geophysical Research: Planets*, *125*(2), e2020JE006599. <https://doi.org/10.1029/2020JE006599>
- Garcia, R. F., Daubar, I. J., Beucler, É., Posiolova, L. V., Collins, G. S., Lognonné, P., et al. (2022). Newly formed craters on Mars located using seismic and acoustic wave data from InSight. *Nature Geoscience*, *15*(10), 774–780. <https://doi.org/10.1038/s41561-022-01014-0>
- Goins, N. R., & Lazarewicz, A. R. (1979). Martian seismicity. *Geophysical Research Letters*, *6*(4), 368–370. <https://doi.org/10.1029/GL006i005p00368>
- Golombek, M. P. (2002). A revision of Mars seismicity from surface faulting. In *33rd annual lunar planetary science conference*. Abstract 1244.
- Golombek, M. P., Banerdt, W. B., Tanaka, K. L., & Tralli, D. M. (1992). A prediction of Mars seismicity from surface faulting. *Science*, *258*(5084), 979–981. <https://doi.org/10.1126/science.258.5084.979>
- Horleston, A. C., Clinton, J. F., Ceylan, S., Giardini, D., Charalambous, C., Irving, J. C. E., et al. (2022). The far side of Mars: Two distant marsquakes detected by InSight. *The Seismic Record*, *2*(2), 88–99. <https://doi.org/10.1785/0320220007>
- InSight Marsquake Service. (2022). *Mars seismic catalogue, InSight mission, V12 2022-10-01*. ETHZ, IPGP, JPL, ICL, Univ. Bristol. <https://doi.org/10.12686/a18>
- Jacob, A., Plasman, M., Perrin, C., Fuji, N., Lognonné, P., Xu, Z., et al. (2022). Seismic sources of InSight marsquakes and seismotectonic context of Elysium Planitia, Mars. *Tectonophysics*, *837*, 229434. <https://doi.org/10.1016/j.tecto.2022.229434>
- Kagan, Y. Y. (2002). Seismic moment distribution revisited: II. Moment conservation principle. *Geophysical Journal International*, *149*(3), 731–754. <https://doi.org/10.1046/j.1365-246x.2002.01671.x>
- Kawamura, T., Clinton, J. F., Zenhäusern, G., Ceylan, S., Horleston, A. C., Dahmen, N. J., et al. (2022). S1222a - The largest Marsquake detected by InSight. *Geophysical Research Letters*, *49*, e2022GL101543. <https://doi.org/10.1029/2022GL101543>
- Kim, D., Banerdt, W. B., Ceylan, S., Giardini, D., Lekić, V., Lognonné, P., et al. (2022). Surface waves and crustal structure on Mars. *Science*, *378*(6618), 417–421. <https://doi.org/10.1126/science.abq7157>
- Knapmeyer, M., Knapmeyer-Endrun, B., Plesa, A.-C., Böse, M., Kawamura, T., Clinton, J. F., et al. (2019). Estimation of the seismic moment rate from an incomplete seismicity catalog, in the context of the InSight Mission to Mars. *Bulletin of the Seismological Society of America*, *109*(3), 1125–1147. <https://doi.org/10.1785/0120180258>
- Knapmeyer, M., Oberster, J., Hauber, E., Wählich, M., Deuchler, C., & Wagner, R. (2006). Working models for spatial distribution and level of Mars' seismicity. *Journal of Geophysical Research*, *111*(E11), E11006. <https://doi.org/10.1029/2006JE002708>
- Knapmeyer, M., & Weber, R. C. (2015). Seismicity and interior structure of the Moon. In V. C. H. Tong & R. A. Garcia (Eds.), *Extraterrestrial Seismology* (pp. 203–224). Cambridge University Press.
- Kostrov, B. V. (1974). Seismic moment and energy of Earthquakes, and seismic flow of rock. *Izvestiya, Academy of Sciences, USSR: Physics of the solid earth*, *10*, 13–21.
- Kremer, C., Haines, J., Holt, W. E., Blewitt, G., & Lavallee, D. (2000). On the determination of a global strain rate model. *Earth Planets and Space*, *52*(10), 765–770. <https://doi.org/10.1186/BF03352279>
- Lognonné, P., Banerdt, W. B., Giardini, D., Pike, W. T., Christensen, U., Laudet, P., et al. (2019). SEIS: InSight's seismic experiment for internal structure of Mars. *Space Science Reviews*, *215*(1), 12. <https://doi.org/10.1007/s11214-018-0574-6>
- McKenzie, D., Jackson, J., & Priestley, K. (2005). Thermal structure of oceanic and continental lithosphere. *Earth and Planetary Science Letters*, *233*(3–4), 337–349. <https://doi.org/10.1016/j.epsl.2005.02.005>
- Phillips, R. J. (1991). Expected rates of marsquakes. LPI Tech Rept. 91-02 LPI/TR-91-02. In *Scientific rationale and requirements for a global seismic network on mars* (pp. 35–38). Lunar and Planetary Institute.
- Plesa, A.-C., Knapmeyer, M., Golombek, M. P., Breuer, D., Grott, M., Kawamura, T., et al. (2018). Present-day Mars' seismicity predicted from 3-D thermal evolution models of interior dynamics. *Geophysical Research Letters*, *45*(6), 2580–2589. <https://doi.org/10.1002/2017GL076124>
- Posiolova, L. V., Lognonné, P., Banerdt, W. B., Clinton, J., Collins, G. S., Kawamura, T., et al. (2022). Largest recent impact craters on Mars: Orbital imaging and surface seismic co-investigation. *Science*, *378*(6618), 412–417. <https://doi.org/10.1126/science.abq7704>
- Shi, Y., & Bolt, B. A. (1982). The standard error of the magnitude-frequency b value. *Bulletin of the Seismological Society of America*, *72*(No. 5), 1677–1687. <https://doi.org/10.1785/bssa0720051677>
- Stähler, S. C., Mittelholz, A., Perrin, C., Kawamura, T., Kim, D., Knapmeyer, M., et al. (2022). Tectonics of Cerberus Fossae unveiled by marsquakes. *Nature Astronomy*, *6*(12), 1376–1386. <https://doi.org/10.1038/s41550-022-01803-y>
- Taylor, J., Teanby, N., & Wookey, J. (2013). Estimates of seismic activity in the Cerberus Fossae region of Mars. *Journal of Geophysical Research*, *118*(12), 2570–2581. <https://doi.org/10.1002/2013JE004469>